The Brayton Cycle Using Real Air and Polytropic Component Efficiencies

W. H. Heiser
Professor of Aeronautics, Emeritus
Life Fellow ASME
Honorary Fellow AIAA

T. Huxley

J. W. Bucey

U.S. Air Force Academy,
CO 80840

This paper presents the results of a fundamental, comprehensive, and rigorous analytical and computational examination of the performance of the Brayton propulsion and power cycle employing real air as the working fluid. This approach capitalizes on the benefits inherent in closed cycle thermodynamic reasoning and the behavior of the thermally perfect gas to facilitate analysis. The analysis uses a high fidelity correlation to represent the specific heat at constant pressure of air as a function of temperature and the polytropic efficiency to evaluate the overall efficiency of the adiabatic compression and expansion processes. The analytical results are algebraic, transparent, and easily manipulated, and the computational results present a useful guidance for designers and users. The operating range of design parameters considered covers any current and foreseeable application. The results include some important comparisons with more simplified conventional analyses. [DOI: 10.1115/1.4003671]

1 Introduction

Many persistent questions about propulsion and power cycles are generally related to the impact of gas properties at elevated temperatures on performance [1,2]. One of the most important questions is whether the variation in gas properties with temperature places any limits on the maximum useful pressures and temperatures of gas turbines. Judging by the abundance of references to the ideal Brayton cycle (IBC) (also known as the ideal air-standard cycle and the ideal Joule cycle) found in the open literature (e.g., Refs. [3–7]), the IBC has provided the fundamental basis for much of the understanding of and reasoning about many devices that convert chemical energy into mechanical work, including stationary ground and marine gas turbine power plants and aircraft gas turbine engines. The purpose of this paper is to examine the Brayton cycle in more realistic terms and to demonstrate that the resulting real air Brayton cycle (RABC) is capable of answering many questions, including important contemporary ones concerning the behavior of power cycles capable of large compression pressure ratios and high combustion temperatures. This analysis is, of course, exact for cycles that directly transfer heat to the air from geothermal, nuclear, or solar sources. The RABC consists of four separate simple processes executed in sequence, as diagramed in Fig. 1. The station numbers used throughout this paper conform to the gas turbine industry standard [8].

The thermal efficiency and mass specific work are of paramount importance to stationary power plants and aircraft engines alike. In every case, the crucial initial step is to convert the chemical energy of the fuel into work that is available to produce power and/or accelerate intake and fuel flows to ultimately produce reaction thrust. Consequently, the thermal efficiency and the mass specific work of the RABC are the primary focus of this investigation. The thermal efficiency and mass specific work of the closed RABC thermodynamic cycle are given by

$$\eta_{\text{th}} = \frac{w}{q_a} = \frac{q_a - q_r}{q_a} = 1 - \frac{q_r}{q_a} \tag{1}$$

The main purpose of this study was to isolate and demonstrate the importance of two physical effects that fit easily into the traditional thermodynamic closed cycle analysis. It is therefore carefully constructed to avoid the complications of combustion reactions, which require the specification of the chemical composition of the fuel, the combustor operation and geometry, and the complex chemical reaction analysis, and inevitably leads to open cycle performance analysis and the introduction of other experiential information such as heat transfer, cooling air sources and distribution, turbine efficiency, and engine cycle parameters (e.g., bypass ratio, fan pressure ratio, and whether the exhaust flows are separate or mixed).

The four simple processes that constitute the RABC are next described in detail in order to improve the understanding of their individual behaviors and to develop analytical models that can be used to provide quantitative results. For the remainder of this investigation, it is assumed that e_c, π_c, e_e, π_e, and T_4/T_0 are known and that $T_0 = 518.7°R$ (288.2 K). Further, all properties have been and will be expressed in either intensive or mass specific terms.

2 Analysis

2.1 The Properties of Real Air. The chemical composition of the representative air used in this paper consists of 79% N_2 and 21% O_2 by moles (or number of molecules). The inclusion of such trace constituents as argon or water will not appreciably affect the results. Air is assumed to be in equilibrium throughout the RABC and is observed to behave as a thermally perfect gas for pressures above 1 atm and for temperatures between $500°R$ and $4000°R$ (277.8 K and 2222 K) (see Sec. 2.6 of Ref. [4] and Sec. 2.5 of Ref. [9]). The chemical composition of air for pressures above 1 atm varies insignificantly for temperatures between $500°R$ and $4000°R$ (whence the gas constant of air is also constant at 0.06854 Btu/lbm°R (0.2870 kJ/(kg K)). In order to facilitate consistency between remote workers, the static conditions at Station 0 usually correspond to the standard atmosphere (see Sec. 2.4 of Ref. [9] and Ref. [10]).

The algebraic correlation of Sec. 2.6 of Ref. [4] was used to calculate the values of the specific heat at constant pressure shown of real air in Fig. 2. These values are within 1% of the exact values over the temperature range of interest. Should greater accuracy be required, thermodynamic equilibrium calculations by means of Gibbs function minimization can be rapidly accomplished (see Chap. 6 of Ref. [9]). It should be noted that C_p increases steadily with temperature but not nearly in proportion to

Contributed by the International Gas Turbine Institute (IGTI) of ASME for publication in the JOURNAL OF ENGINEERING FOR GAS TURBINES AND POWER. Manuscript received December 3, 2010; final manuscript received February 7, 2011; published online May 17, 2011. Editor: Dilip R. Ballal.

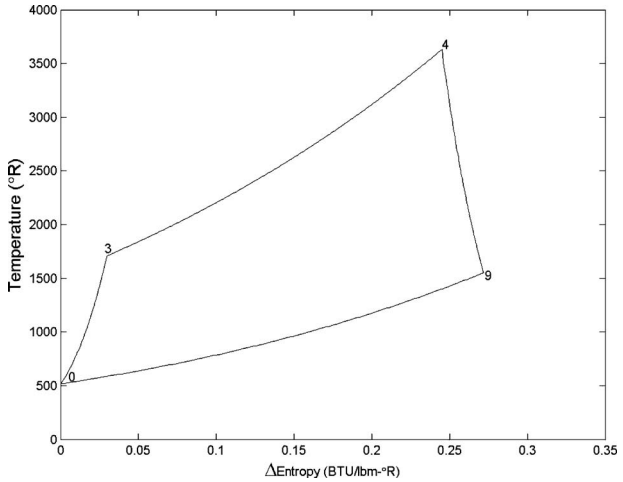

Fig. 1 A typical RABC thermodynamic cycle, showing the four simple processes and station numbering. For this cycle, $\pi_c = 50$, $T_4/T_0 = 7.0$, $e_c = 0.90$, and $e_e = 0.90$.

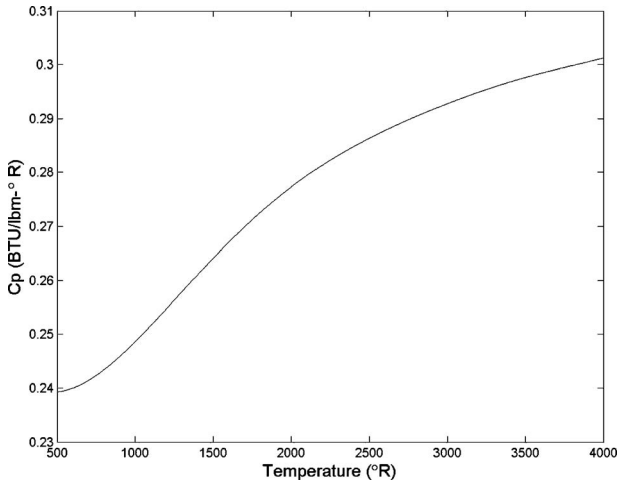

Fig. 2 Plot of the specific heat at constant pressure of real air versus absolute temperature for static pressures greater than 1 atm and temperatures between 500° *R* and 4000° *R*

the absolute temperature, so that the ratio T/C_p increases almost linearly with absolute temperature. Since real air behaves as an ideal or perfect gas under all anticipated conditions, only the gas constant and the specific heat are needed to calculate the remaining thermodynamic coefficients, such as the specific heat at constant volume and the ratio of specific heats [3].

2.2 The RABC Adiabatic Compression Process (Station 0 to Station 3). The RABC compression process is modeled as adiabatic, and the inevitable irreversibility of the work interaction is modeled by constant polytropic efficiency [3,4]. Any compression resulting from the deceleration of the freestream flow is included in the overall process (i.e., points 0–3) [3,4]. The freestream compression in flight is primarily a function of Mach number and can be substantial, the isentropic compression pressure ratio being about 1.89 for a Mach number of 1. The polytropic efficiency is best described as the efficiency of a differential or infinitesimal pressure change and therefore represents the established level of technological capability rather than the demonstrated performance of an entire device. Since the compression produces a finite pressure change, the overall efficiency decreases with compression pressure ratio and is always less than the polytropic efficiency. The reverse is true for the expansion process [3,4].

The definition of compression polytropic efficiency and the Gibbs differential equation can be combined to show that [3,4]

$$dT = \frac{RT}{e_c C_{pc}} \cdot \frac{dP}{P} \tag{2}$$

Since the coefficient on the right hand side of Eq. (2) depends only on temperature, Eq. (2) can be integrated numerically over the entire pressure range to find

$$T_3 = T_0 + \frac{R}{e_c} \int_{P_0}^{\pi_c P_0} \frac{T}{C_{pc}} \cdot \frac{dP}{P} \tag{3}$$

which can be combined with the constant specific heat version of Eq. (3),

$$\ln\left(\frac{T_3}{T_0}\right) = \frac{R}{e_c \overline{C_{pc}}} \cdot \ln(\pi_c) \tag{4}$$

to allow the derived specific heat for the adiabatic compression process to be evaluated from the equation

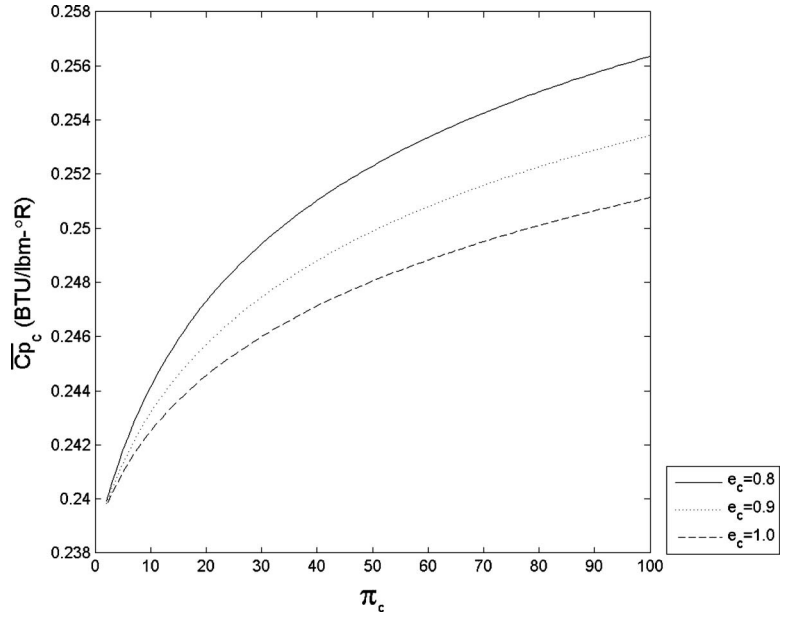

Fig. 3 Plot of $\overline{C_{pc}}$ as a function of π_c and e_c

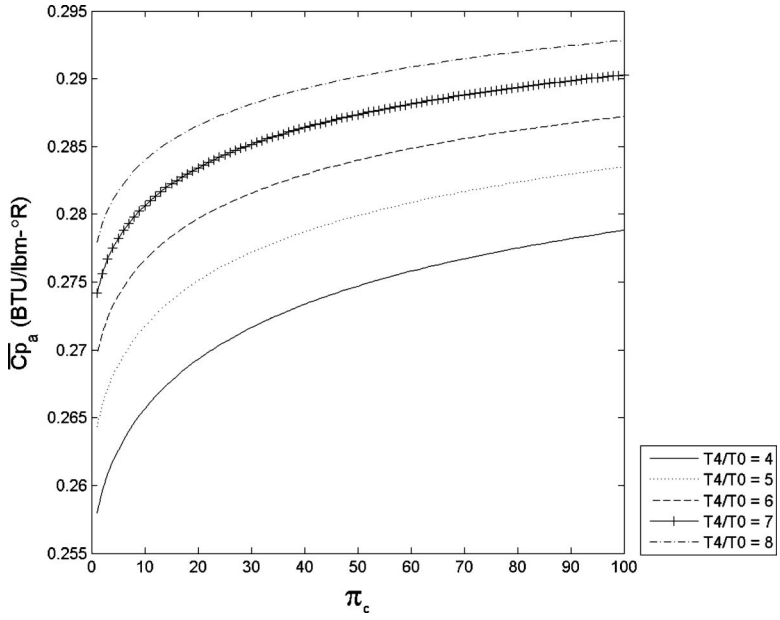

Fig. 4 Plot of $\overline{C_{pa}}$ as a function of π_c and T_4/T_0 for e_c=0.90

$$\overline{C_{pc}} = \frac{R}{e_c} \cdot \frac{\ln(\pi_c)}{\ln\left(\frac{T_3}{T_0}\right)} \tag{5}$$

Figure 3 presents the results of computations of $\overline{C_{pc}}$ based on Eqs. (3) and (5) for the range of $1 < \pi_c < 100$. It should be noted that $\overline{C_{pc}}$ depends on e_c but is independent of T_4/T_0 because the compression process precedes the heat addition process and that $\overline{C_{pc}}$ varies slowly at the highest values of π_c for any value of e_c primarily because the temperature at the end of the compression process changes slowly as π_c increases. These results highlight the fact that $\overline{C_{pc}}$ is dependent on e_c, and this would affect the succeeding processes. In order to avoid associated complications, it will be assumed hereinafter that e_c=0.9 because that value is representative of contemporary technology (e.g., p. 107 of Ref. [11]).

From this point on, a careful distinction must be drawn between the derived value of $\overline{C_p}$ that is appropriate for an entire simple process and the particular value of C_p that corresponds to the prevailing absolute temperature of the air. The former are derived from the latter. It is evident from the derivation of $\overline{C_{pc}}$ that it is not an average value of C_p over the adiabatic compression process.

2.3 The RABC Heat Addition Process (Station 3 to Station 4). The RABC combustion process is modeled as simple, constant pressure heat addition [3,4,11]. The pressure may be taken to be constant in the combustor because the designer reduces the velocity as much as possible in order to support the combustion process by increasing the pressure, temperature, and residence time, so that the resulting pressure losses are negligible.

Since

$$q_a = \int_{T_3}^{T_4} C_{pa} dT \tag{6}$$

then the derived specific heat for the heat addition process is

$$\overline{C_{pa}} = \frac{\int_{T_3}^{T_4} C_{pa} dT}{(T_4 - T_3)} = \frac{q_a}{(T_4 - T_3)} \tag{7}$$

Equation (7) can be integrated either numerically or analytically (using the algebraic correlation of Sec. 2.6 of Ref. [4]). Equation (7) reveals that $\overline{C_{pa}}$ is equal to the temperature averaged value of C_p over the temperature range of the integral.

Figure 4 presents the results of computations of $\overline{C_{pa}}$ based on Eqs. (3), (6), and (7) for the ranges of $1 < \pi_c < 100$ and $4 < T_4/T_0 < 8$. It should be noted that $\overline{C_{pa}}$ depends also upon e_c because the compression process precedes the heat addition process and that $\overline{C_{pa}}$ varies slowly at the highest values of π_c for any value of T_4/T_0 primarily because the temperature at the end of the compression process changes slowly as π_c increases. Nevertheless, $\overline{C_{pa}}$ varies with T_4/T_0 because of the strong dependence of C_p on temperature (see Fig. 2).

It is tempting at this point to include factors that represent losses in the heat addition process resulting from either the incomplete combustion of the fuel or from the pressure drops within the combustor necessary for the mixing of reactants and products. However, these losses are insignificant in modern machines, and the complexity required for their inclusion is not worth the small improvement in accuracy.

2.4 The RABC Adiabatic Expansion Process (Station 4 to Station 9). The RABC expansion process is modeled as adiabatic, and the inevitable irreversibility of the work interaction is modeled by constant polytropic efficiency [3,4]. Any expansion taking place in components designed to convert the cycle work to another useful form, such as power turbines or nozzles, is included in the overall process. The expansion pressure ratio is defined here as the pressure at Station 4 divided by the pressure at Station 9, and therefore exceeds 1.

The definition of expansion polytropic efficiency and the Gibbs differential equation can be combined to show that [3,4]

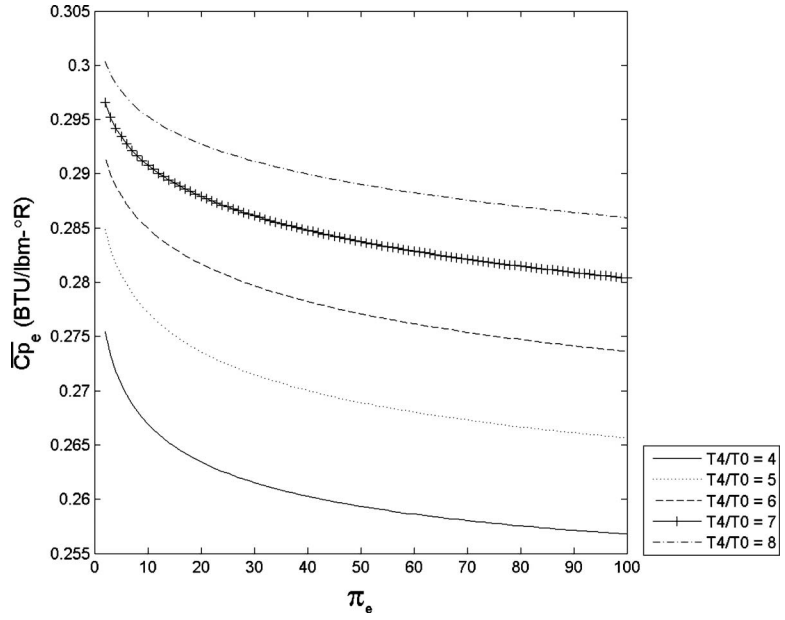

Fig. 5 Plot of $\overline{C_{pe}}$ as a function of π_e and T_4/T_0 for $\pi_e=\pi_c$ and $e_c=e_e=0.90$

$$dT = \frac{e_e RT}{C_{pe}} \cdot \frac{dP}{P} \tag{8}$$

Since the coefficient on the right hand side of Eq. (8) depends only on temperature, Eq. (8) can be integrated numerically over the entire pressure range to find

$$T_4 = T_9 + e_e R \int_{P_0}^{\pi_e P_0} \frac{T}{C_{pc}} \cdot \frac{dP}{P} \tag{9}$$

which can be combined with the constant specific heat formulation of Eq. (9) to allow the evaluation of the derived specific heat for the adiabatic expansion process from the equation

$$\overline{C_{pe}} = e_e R \cdot \frac{\ln(\pi_e)}{\ln\left(\frac{T_4}{T_9}\right)} \tag{10}$$

It is evident from the derivation of $\overline{C_{pe}}$ that it is not an average value of C_p over the adiabatic expansion process.

Figure 5 presents the results of computations of $\overline{C_{pe}}$ based on Eqs. (9) and (10) for the ranges of $1<\pi_e<100$ and $4<T_4/T_0<8$. It should be noted that $\overline{C_{pe}}$ depends on π_c, e_c, e_e, and T_4/T_0 because the expansion process follows both the compression process and the heat addition process. $\overline{C_{pe}}$ varies slowly at the highest values of π_e for any value of T_4/T_0 primarily because the temperature at the end of the expansion process changes slowly as π_e increases. Nevertheless, $\overline{C_{pe}}$ varies with T_4/T_0 because of the strong dependence of C_p on temperature (see Fig. 2). As in the case of the compression process, it has been assumed for the expansion process that $e_e=0.9$ because that value is representative of contemporary technology (e.g., p. 107 of Ref. [11]). It has also been assumed that $\pi_e=\pi_c$ for reasons given below.

2.5 The RABC Heat Rejection Process (Station 9 to Station 0). The RABC heat rejection process is modeled as simple, constant pressure heat transfer [3,4,9]. The constant pressure assumption is justifiable because the air is immersed in the constant static pressure ambient surroundings during this process. Applying conservation of momentum to the exhaust stream control volume during the heat rejection process reveals that the momentum of the air and hence the thrust do not change during this process.

Since

$$q_r = \int_{T_0}^{T_9} C_{pr} dT \tag{11}$$

then the derived specific heat for the heat addition process is given by the expression

$$\overline{C_{pr}} = \frac{\int_{T_0}^{T_9} C_{pr} dT}{(T_9 - T_0)} = \frac{q_r}{(T_9 - T_0)} \tag{12}$$

Equation (11) can be integrated either numerically or analytically (using the algebraic correlation of Sec. 2.6 of Ref. [4]). Equation (12) reveals that $\overline{C_{pr}}$ is equal to the temperature averaged value of C_p over the temperature range of the integral.

Figure 6 presents the results of calculations of $\overline{C_{pr}}$ based on Eqs. (9), (11), and (12) for the ranges of $1<\pi_e<100$ and $4<T_4/T_0<8$. It should be noted that $\overline{C_{pr}}$ depends on π_c, e_c, π_e, e_e, and T_4/T_0 because the heat rejection process follows the compression process, the heat addition process, and the expansion process. $\overline{C_{pr}}$ varies slowly at the highest values of π_e for any value of T_4/T_0 primarily because the temperature at the end of the expansion process changes slowly as $\pi_e=\pi_c$ increases. Nevertheless, $\overline{C_{pr}}$ varies with T_4/T_0 because of the strong dependence of C_p on temperature (see Fig. 2).

It should be noted that the procedures described above do not require iteration and that the constant pressure models for heat addition and rejection render $\pi_e=\pi_c$, so that only π_c appears in the relationships that follow.

2.6 The RABC T-s Diagram. Once the temperatures at the end points of the four simple processes have been determined by the methods described above, the entire RABC T-s diagram can be computed and drawn by integrating the differential equations listed next, the derivations of which are based on the definitions of polytropic efficiency and the Gibbs differential equation,

$$\left(\frac{ds}{dT}\right)_c = (1 - e_c)\frac{C_{pc}}{T} \tag{13}$$

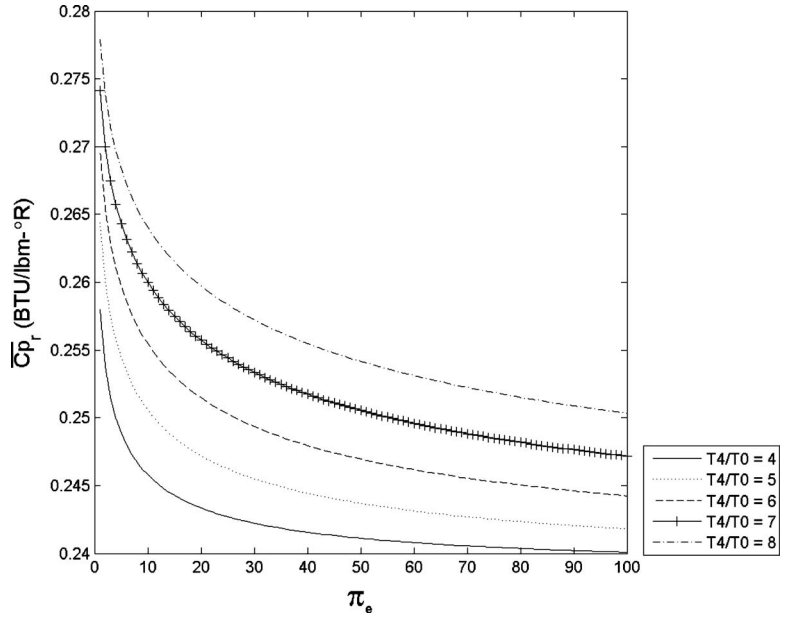

Fig. 6 Plot of $\overline{C_{pr}}$ as a function of $\pi_e=\pi_c$ and T_4/T_0 for $e_c=e_e=0.90$

$$\left(\frac{ds}{dT}\right)_a = \frac{C_{pa}}{T} \tag{14}$$

$$\left(\frac{ds}{dT}\right)_e = \left(1-\frac{1}{e_e}\right)\frac{C_{pe}}{T} \tag{15}$$

$$\left(\frac{ds}{dT}\right)_r = \frac{C_{pr}}{T} \tag{16}$$

Since C_p/T is a thermodynamic property of air that decreases with temperature (see Fig. 2), all four of the simple process lines bend upward with increasing temperature. The typical RABC of Fig. 1 is based on the results of the four simple process calculations described earlier and Eqs. (13)–(16), with $\pi_c=50$, $T_4/T_0=7.0$, $e_c=0.90$, and $e_e=0.90$. The Gibbs differential equation for entropy can be integrated in closed form around the RABC to prove that the T-s diagram of Fig. 1 must close perfectly (i.e., return to the starting point).

3 RABC Results

3.1 RABC Thermal Efficiency. Equations (1), (7), and (12) can be combined to show that the cycle thermal efficiency is given by the expression

$$\eta_{\text{th}} = 1 - \frac{\overline{C_{pr}}}{C_{pa}}\left[\frac{\frac{T_9}{T_4}\cdot\frac{T_4}{T_0}-1}{\frac{T_4}{T_0}-\frac{T_3}{T_0}}\right] \tag{17}$$

provided that the derived specific heats of heat addition and rejection and the temperature ratios correspond to the selected values of compression pressure ratio and peak heat addition temperature. Equation (17) highlights the fact that the thermal efficiency of the RABC is entirely thermodynamic in the sense that it depends only upon absolute temperatures. It is therefore thermodynamically correct to view the adiabatic compression process solely in terms of the temperature increase (rather than the pressure increase) that it creates.

Similarly, Eqs. (5), (10), and (17) can be rearranged and combined to yield

$$\eta_{\text{th}} = 1 - \frac{\overline{C_{pr}}}{C_{pa}}\left[\frac{\pi_c^{-(e_e R/\overline{C_{pe}})}\cdot\frac{T_4}{T_0}-1}{\frac{T_4}{T_0}-\pi_c^{(R/e_c\overline{C_{pc}})}}\right] \tag{18}$$

Equation (18) can be used to calculate the RABC thermal efficiency and thereby reveal the general behavior of the RABC. This convenient algebraic relationship separates and exposes the separate influence of each of the contributing factors and is easily manipulated to achieve other desirable ends. It also confirms that use of polytropic efficiencies and derived specific heats makes the behavior of the RABC transparent. The thermal efficiency of the RABC of Fig. 1 obtained from Eq. (18) is 0.514.

Figure 7 presents an extensive set of computations of RABC thermal efficiency based on the values of the derived specific heats shown in Figs. 3–6. The general features of Fig. 7 have been previously observed and documented (e.g., Ref. [2]), some of which can be understood by imagining a series of T-s diagrams and applying Eq. (1). On the one hand, as the adiabatic compression pressure ratio approaches one from above, the heat added approaches the heat rejected and the thermal efficiency approaches zero (see Eq. (1)). On the other hand, as the temperature at the end of compression approaches the peak cycle temperature from below, the heat added approaches zero while the heat rejected increases and the thermal efficiency becomes negative and arbitrarily large (see Eq. (1)). Consequently, both the maximum RABC efficiency and a thermal efficiency of zero must occur sequentially before the temperature at the end of compression reaches the peak cycle temperature. This reasoning is confirmed, for example, by the curve in Fig. 7 for $T_4/T_0=4$, which shows that the maximum thermal efficiency occurs where the temperature ratio at the end of compression is approximately 2.7 and passes through a thermal efficiency of zero where the temperature ratio at the end of compression is approximately 3.6. Again, it is the absolute temperatures that matter. These features appear in Fig. 7, as well as the tendency of the maximum RABC thermal efficiency to increase as the compression pressure ratio and peak heat addition temperature are increased. Figure 7 also reveals that there is a law of diminishing returns at work, for which the potential improvements in RABC thermal efficiency become less as the compression pressure ratio and peak heat addition temperature are in-

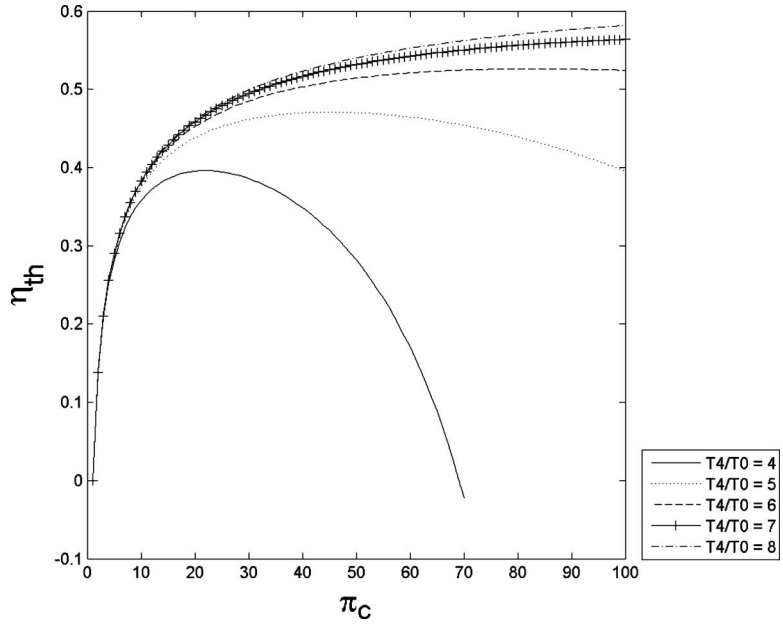

Fig. 7 Plot of the thermal efficiency of the RABC as a function of π_c and T_4/T_0 for $e_c = e_e = 0.90$

creased. Many studies have shown that the need for increasing amounts of compressed air to cool the turbines as the compression pressure ratio and peak heat addition temperature increase further diminishes the thermal efficiency. Consequently, the thermal efficiencies shown in Fig. 7 should also be regarded as increasingly optimistic as the compression pressure ratio and peak heat addition temperature increase because of high temperature material limitations.

Two examples based on Eq. (18) are presented below in order to illustrate its consequences and versatility. Many variations on these and other themes are possible.

3.1.1 Example 1: Sensitivity Analyses. The sensitivity of thermal efficiency to variations of the derived specific heats at constant pressure can be found by differentiating Eq. (18) to find that

$$\frac{\partial \eta_{\text{th}}}{\partial \overline{C_{pc}}} = (1 - \eta_{\text{th}}) \frac{\dfrac{R}{e_c \overline{C_{pc}}^2} \cdot \ln(\pi_c)}{\left(\pi_c^{-(R/e_c \overline{C_{pc}})} \dfrac{T_4}{T_0} - 1 \right)} \tag{19}$$

$$\frac{\partial \eta_{\text{th}}}{\partial \overline{C_{pa}}} = \frac{(1 - \eta_{\text{th}})}{\overline{C_{pa}}} \tag{20}$$

$$\frac{\partial \eta_{\text{th}}}{\partial \overline{C_{pe}}} = (\eta_{\text{th}} - 1) \frac{\dfrac{T_4}{T_0} \cdot \dfrac{e_e R}{\overline{C_{pe}}^2} \cdot \ln(\pi_c)}{\left(\dfrac{T_4}{T_0} - \pi_c^{(e_e R/\overline{C_{pe}})} \right)} \tag{21}$$

$$\frac{\partial \eta_{\text{th}}}{\partial \overline{C_{pr}}} = \frac{(\eta_{\text{th}} - 1)}{\overline{C_{pr}}} \tag{22}$$

Since the sum of the absolute numerical values of the partial differentials calculated from Eqs. (19)–(22) is less than about 10 for typical RABC conditions, it follows that the derived specific heats must be known within about 0.4% in order to evaluate thermal efficiency within 0.01 (or 1%) from Eq. (18), provided that the adiabatic compression and expansion polytropic efficiencies are known. This sensitivity led to stringent convergence requirements on the computation of the $\overline{C_p}$ values presented in Figs. 3–6. Despite the apparently smooth behavior of the curve of Fig. 2, the commercial MATLAB program required that the simple processes be divided into at least 40,000 equal steps in order to achieve the desired $\overline{C_p}$ accuracy through the integration of Eqs. (3), (6), (9), and (11). The $\overline{C_p}$ values shown in Figs. 3–6 are within about 0.2% of their values found after 1×10^6 equal steps, the latter being presumed to be exact because they were no longer changing.

3.1.2 Example 2: The Single Value of $\overline{C_p}$ That Yields the Correct RABC Thermal Efficiency. Equation (18) can be used to calculate a single value of $\overline{C_p}$ for all four simple processes that can be used to produce the correct RABC thermal efficiency for any given set of operating conditions. This is accomplished by setting the thermal efficiency to the value found from a complete calculation and by finding the single $\overline{C_p}$ by iteration that will give the identical result in Eq. (18). In order to understand the consequences of this approach, consider the three typical operating points:

point A: $\pi_c = 50, \quad T_4/T_0 = 4.0, \quad e_c = 0.90, \quad e_e = 0.90$

point B: $\pi_c = 50, \quad T_4/T_0 = 6.0, \quad e_c = 0.90, \quad e_e = 0.90$

point C: $\pi_c = 100, \quad T_4/T_0 = 8.0, \quad e_c = 0.90, \quad e_e = 0.90$

The results of the operations described above are

point A: $\eta_{\text{th}} = 0.282, \quad \overline{C_p}$
$= 0.253$ Btu/lbm °R or 1.059 kJ/(kg K)

point B: $\eta_{\text{th}} = 0.514, \quad \overline{C_p}$
$= 0.268$ Btu/lbm °R or 1.122 kJ/(kg K)

point C: $\eta_{\text{th}} = 0.582, \quad \overline{C_p}$
$= 0.275$ Btu/lbm °R or 1.151 kJ/(kg K)

The quoted values of η_{th} agree with those of Fig. 7, even the very low value of point A. These results suggest that the variation in C_p with the temperature of air affects every aspect of RABC performance. On the one hand, these results show that the single value of $\overline{C_p}$ depends strongly on the cycle operating conditions. On the

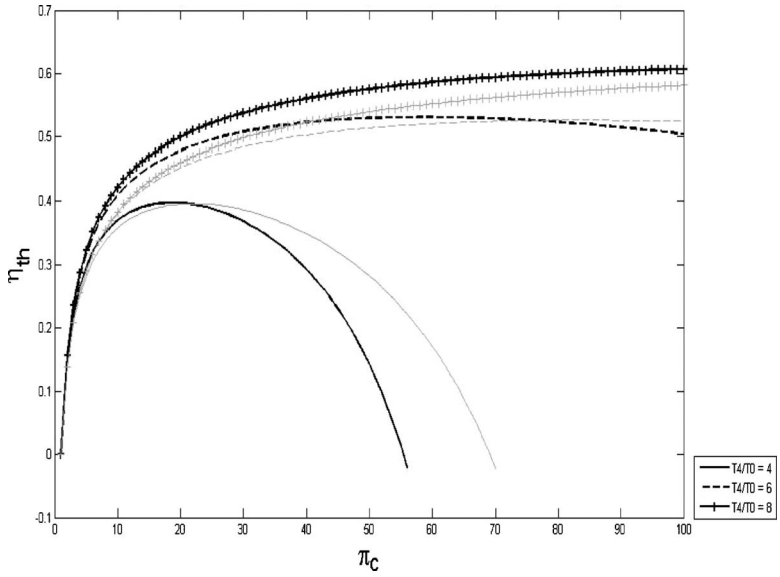

Fig. 8 Plots of the thermal efficiency as a function of π_c and T_4/T_0 for the RABC and for the Brayton cycle with constant C_p=0.240 Btu/lbm°R for $e_c = e_e$=0.90. The thermal efficiency of the RABC is shown in lighter lines, and that of the constant C_p Brayton cycle is shown in darker lines.

other hand, Fig. 8 shows that the behavior of the thermal efficiency of the RABC is quite different from that of the Brayton cycle with constant C_p=0.240 Btu/lbm°R (1.005 kJ/(kg K)). The information found in Fig. 8 reveals, for example, that both the optimum π_c for a given T_4/T_0 and the η_{th} for a given π_c and T_4/T_0 are significantly different between the RABC and the constant C_p Brayton cycle. The choice of C_p=0.240 Btu/lbm°R in this and later examples is based solely on the fact that this value is very frequently used in the open literature.

3.2 Dimensionless RABC Mass Specific Work $w/C_{p0}T_0$. There is equal interest in the net mass specific work of the RABC [5–7] because this quantity determines the required size of the machine. Equations (1), (5), and (7) can be combined to show that the RABC dimensionless mass specific work is given by the expression

$$\frac{w}{C_{p0}T_0} = \frac{\overline{C_{pa}}}{C_{p0}} \cdot \left(\frac{T_4}{T_0} - \frac{T_3}{T_0}\right) \cdot \eta_{\text{th}} = \frac{\overline{C_{pa}}}{C_{p0}} \cdot \left(\frac{T_4}{T_0} - \pi_c^{R/e_c\overline{C_{pc}}}\right) \cdot \eta_{\text{th}} \tag{23}$$

Equation (23) highlights the fact that the dimensionless mass specific work of the RABC is entirely thermodynamic in the sense that it depends only upon absolute temperatures.

Figure 9 shows the results of computations based on Eq. (23) that reveal that the dimensionless mass specific work $w/C_{p0}T_0$ of

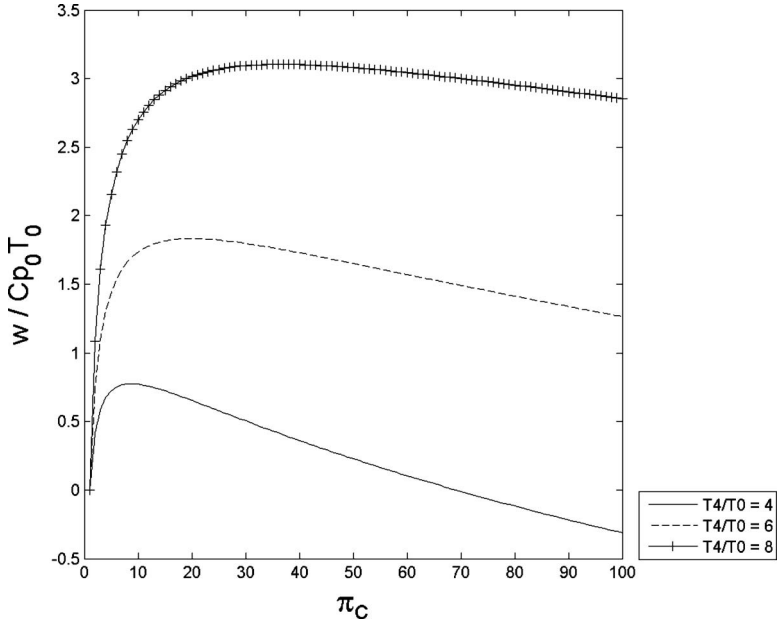

Fig. 9 Plot of the dimensionless mass specific work of the RABC as a function of π_c and T_4/T_0 for $e_c = e_e$=0.90

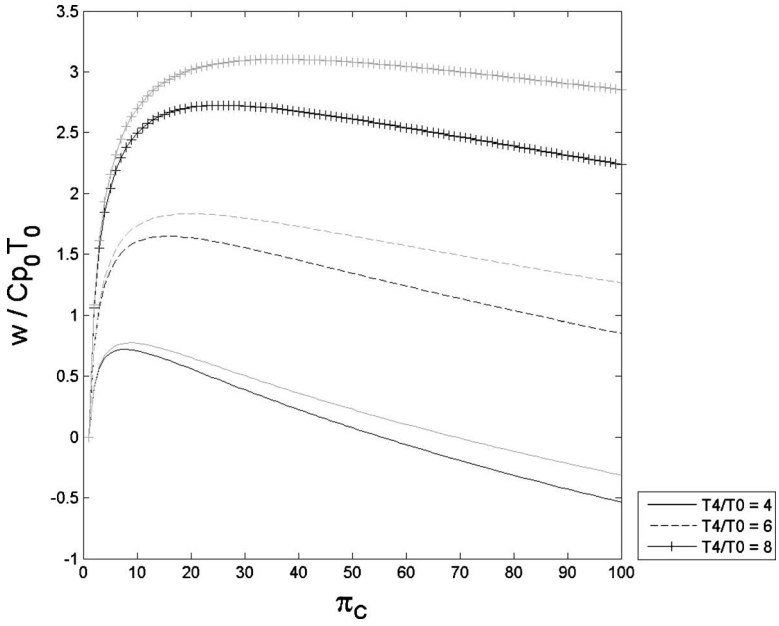

Fig. 10 Plots of the dimensionless mass specific work as a function of π_c and T_4/T_0 for the RABC and the Brayton cycle with constant C_p =0.240 Btu/lbm°R for $e_c = e_e = 0.90$. The dimensionless mass specific work of the RABC is shown in lighter lines, and that of the constant C_p Brayton cycle is shown in darker lines.

the RABC increases rapidly with heat added (or T_4/T_0) and that the optimum π_c is significantly less than those found in Fig. 7 corresponding to optimum thermal efficiency. These conflicts will inevitably require designers to consider compromises that split the difference, especially because RABC dimensionless mass specific work steadily diminishes as π_c increases (see Fig. 9) and RABC thermal efficiency can fall off quickly at the lower values of π_c (see Fig. 7).

Three examples based on Eq. (23) are presented below in order to illustrate its consequences and versatility. Many variations on these and other themes are possible.

3.2.1 Example 1: The Optimum Compression Pressure Ratio for a Given T_4/T_0 . After estimating reasonable, constant (but not necessarily equal) values of $\bar{C}_p$ for the four simple processes from Figs. 3–6, Eq. (23) can be differentiated at constant T_4/T_0 to show that the compression pressure ratio that yields the highest dimensionless RABC mass specific work occurs when

$$\pi_c = \left(\frac{\overline{C_{pr}}}{\overline{C_{pa}}} \cdot \frac{T_4}{T_0} \right)^{1/(1+e_c e_e(\overline{C_{pc}}/\overline{C_{pe}}))\cdot(e_c \overline{C_{pc}}/R)} \tag{24}$$

The results found from Eq. (24) are consistent with those of Fig. 9.

3.2.2 Example 2: The Maximum Dimensionless Mass Specific Work for a Given T_4/T_0 . The value of π_c obtained from Eq. (24) can be substituted into Eq. (23) to estimate the highest RABC dimensionless mass specific work for the given T_4/T_0. These results are also consistent with Fig. 9. Inspection of Eq. (23) reveals that the dimensionless RABC work increases rapidly as heat addition (or T_4/T_0) increases, and inspection of Eq. (24) shows that the optimum compression pressure ratio also increases with T_4/T_0. Both of these trends are evident in the computations presented in Fig. 9.

3.2.3 Example 3: The Single Value of $\overline{C_p}$ That Yields the Correct RABC Dimensionless Mass Specific Work. Equation (23) can be used to calculate a single value of $\overline{C_p}$ for all four simple processes that can be used to produce the correct RABC dimensionless mass specific work for any given set of operating conditions. This is accomplished by setting the dimensionless mass specific work to the value found from the complete calculation and finding the single $\overline{C_p}$ by iteration that will give the identical result in Eq. (23). In order to understand the consequences of this approach, consider the three typical operating points:

point D: $\pi_c = 10, \quad T_4/T_0 = 4.0, \quad e_c = 0.90, \quad e_e = 0.90$

point E: $\pi_c = 20, \quad T_4/T_0 = 6.0, \quad e_c = 0.90, \quad e_e = 0.90$

point F: $\pi_c = 40, \quad T_4/T_0 = 8.0, \quad e_c = 0.90, \quad e_e = 0.90$

The results of the operations described above are

point D: $w/C_{p0}T_0 = 0.772, \quad \overline{C_p}$
$= 0.255$ Btu/lbm°R or 1.068 kJ/(kg K)

point E: $w/C_{p0}T_0 = 1.833, \quad \overline{C_p}$
$= 0.266$ Btu/lbm°R or 1.114 kJ/(kg K)

point F: $w/C_{p0}T_0 = 3.100, \quad \overline{C_p}$
$= 0.274$ Btu/lbm°R or 1.147 kJ/(kg K)

The results plotted in Fig. 10 show that the behavior of the dimensionless mass specific work of the RABC is quite different from that of the Brayton cycle with constant C_p =0.240 Btu/lbm°R. The information of Fig. 10 reveals that the optimum π_c for a given T_4/T_0 and the dimensionless mass specific work for a given set of π_c and T_4/T_0 are both significantly different between the RABC and the constant C_p Brayton cycle.

4 Conclusions

This fundamental study of the RABC has yielded several interesting results. Some of the most important are summarized below.

- This approach has achieved its primary goal of producing

algebraic results that are accessible, transparent, and easily applied for the RABC, a more complex version of the Brayton cycle.
- The use of a high fidelity correlation to represent the specific heat at constant pressure of air as a function of temperature, the derived values of $\overline{C_p}$ to represent each of the four simple processes, and the polytropic efficiency to evaluate the overall efficiency of the adiabatic compression and expansion processes has improved the quality of the results without increasing the complexity of the analysis.
- The cycle thermal efficiency and dimensionless mass specific work are purely thermodynamic quantities in the sense that they depend only upon the absolute temperature distribution throughout the cycle.
- The variation in the specific heat at constant pressure of air for contemporary propulsion and power cycles has a major impact on the cycle thermal efficiency and dimensionless mass specific work that must be taken into account in order to produce accurate results.
- The RABC thermal efficiency generally increases with compression pressure ratio and peak cycle temperatures, but the benefits diminish rapidly as compression pressure ratio and peak cycle temperatures approach their highest probable values.
- The RABC dimensionless mass specific work increases rapidly with peak cycle temperature at any compression pressure ratio, but the optimum compression pressure ratio is relatively low.
- The two preceding observations inevitably lead to the conclusion that the RABC designer will be driven to choose moderate compression pressure ratios and high peak cycle temperatures.
- Conventional analyses employing a fixed specific heat at constant pressure can regrettably lead to different and misleading conclusions.

Acknowledgment

The authors are appreciative of the financial support provided to this project by the Department of Aeronautics (DFAN) of the U.S. Air Force Academy, for the productive climate created by DFAN and the Aeronautics Laboratory, for the helpful advice and technical guidance provided by the faculty, and for the competent administrative support provided by the Digital Consultant Services, Inc.

Nomenclature

C_p = specific heat at constant pressure at a given absolute temperature, Btu/lbm°R or kJ/(kg K)
$\overline{C_p}$ = derived specific heat at constant pressure for an entire simple process, Btu/lbm°R or kJ/(kg K)
e = adiabatic process polytropic efficiency
P = absolute pressure, lbf/ft^2 or Pa
q = mass specific heat exchanged with the thermodynamic cycle, Btu/lbm or kJ/kg
R = gas constant, Btu/lbm°R or kJ/(kg K)
s = mass specific entropy, Btu/lbm°R or kJ/(kg K)
T = absolute temperature, °R or K
w = mass specific work generated by the thermodynamic cycle, Btu/lbm or kJ/kg
η_{th} = thermal efficiency of the thermodynamic cycle
π = compression or expansion pressure ratio

Subscripts

a = simple heat addition process
c = simple adiabatic compression process
e = simple adiabatic expansion process
r = simple heat rejection process
0 = start of the adiabatic compression process and end of the heat rejection process, also freestream conditions
3 = start of heat addition process and end of the adiabatic compression process
4 = start of the adiabatic expansion process and end of the heat addition process
9 = start of the heat rejection process and end of the adiabatic expansion process

References

[1] Wilcock, R. C., Young, J. B., and Horlock, J. H., 2002, "Gas Properties as a Limit to Gas Turbine Performance," ASME Paper No. GT-2002-30517.
[2] Guha, A., 2001, "Performance and Optimization of Gas Turbines With Real Gas Effects," Proc. Inst. Mech. Eng., Part A, **215**, pp. 507–512.
[3] Oates, G. C., 1997, *The Aerothermodynamics of Gas Turbine and Rocket Propulsion* (AIAA Education Series), 3rd ed., AIAA, Reston, VA.
[4] Mattingly, J. D., 2005, *Elements of Propulsion, Gas Turbines and Rockets* (AIAA Education Series), AIAA, Reston, VA.
[5] Sonntag, R. E., 1982, *Introduction to Thermodynamics, Classical and Statistical*, 2nd ed., Wiley, New York.
[6] Cengel, Y., and Boles, M., 1989, *Thermodynamics: An Engineering Approach*, 6th ed., McGraw-Hill, New York.
[7] Boyce, M. P., 2006, *Gas Turbine Engineering Handbook*, 3rd ed., Elsevier, Boston.
[8] SAE, 1974, "Gas Turbine Engine Performance Station Identification and Nomenclature," Society of Automotive Engineers, Aerospace Recommended Practice (ARP), Report No. 755A.
[9] Heiser, W. H., and Pratt, D. T., 1994, *Hypersonic Airbreathing Propulsion* (AIAA Education Series), AIAA, Washington, DC.
[10] 1976, *U.S. Standard Atmosphere, 1976*, U.S. Government Printing Office, Washington, DC.
[11] Mattingly, J. D., Heiser, W. H., and Pratt, D. T., 2002, *Aircraft Engine Design* (AIAA Education Series), 2nd ed., AIAA, Reston, VA.